General Disclaimer

One or more of the Following Statements may affect this Document

- This document has been reproduced from the best copy furnished by the organizational source. It is being released in the interest of making available as much information as possible.

- This document may contain data, which exceeds the sheet parameters. It was furnished in this condition by the organizational source and is the best copy available.

- This document may contain tone-on-tone or color graphs, charts and/or pictures, which have been reproduced in black and white.

- This document is paginated as submitted by the original source.

- Portions of this document are not fully legible due to the historical nature of some of the material. However, it is the best reproduction available from the original submission.

NASA Technical Memorandum 78581

Computation of Turbulent Near Wake for Asymmetric Airfoils

George S. Deiwert

March 1979

National Aeronautics and
Space Administration

NASA Technical Memorandum 78581

Computation of Turbulent Near Wake for Asymmetric Airfoils

George S. Deiwert, Ames Research Center, Moffett Field, California

National Aeronautics and
Space Administration

Ames Research Center
Moffett Field, California 94035

COMPUTATION OF TURBULENT NEAR WAKE FOR ASYMMETRIC AIRFOILS

George S. Deiwert
Ames Research Center, NASA
Moffett Field, California 94035, USA

Summary

A numerical procedure for studying the turbulent near wake of two-dimensional airfoil sections is presented. The Reynolds averaged Navier-Stokes equations are written for flow about bodies of arbitrary geometry and solved on an arbitrary nonuniform curvilinear computational mesh. Eddy viscosity and Reynolds stress turbulence transport models are considered. Specific examples are shown for the RAE 2814 airfoil section by using an algebraic eddy viscosity model with streamwise relaxation and the interactive Reynolds stress model proposed by Bradshaw.

Symbols

c	chord length
c_p	specific heat at constant pressure
$\vec{e}$	unit vector in Cartesian space
c_v	specific internal energy
$\vec{n}$	unit outward normal vector
p	pressure
S	surface area
T	temperature
t	time
u,v	Cartesian velocity components
vol	volume element of fluid
γ	isentropic exponent
δ	boundary layer thickness
μ	coefficient of molecular viscosity
ρ	mass density

Subscripts

BL	boundary layer model
DS	evaluated at dividing streamline
ℓ	laminar

te trailing edge

w wall

WK wake model

δ evaluated at boundary layer edge

Superscripts

$\hat{}$ curvilinear space component

$'$ fluctuating component

Introduction

The prediction of flow fields over airfoil sections with viscous-inviscid interactions has received considerable attention over the past several years. One region of particular concern is the trailing edge of the airfoil where predictions have been most difficult. In this region, the interaction in the near wake of the two turbulent shear layers from the upper and lower surfaces with one another is important. Each shear layer experiences a different flow history and, in the near-wake region, will sustain normal pressure gradients. The turbulent mixing process in the near wake is not yet well understood. Simplified numerical analyses initiated just at the trailing edge, not accounting for normal pressure gradients, may be inadequate regardless of the degree of sophistication of the turbulence transport model used.

In this study, the two-dimensional Reynolds averaged compressible Navier-Stokes equations are used to describe the entire flow field. In this way, it is possible to account for both the upstream history of the shear layers and the viscous-inviscid interaction at the trailing edge. Differential turbulent transport models can be used to describe the Reynolds stresses in the attached shear layers and their carry-over into the free shear flow of the wake.

Both eddy viscosity and Reynolds stress turbulence transport models are considered. Because the eddy viscosity models relate turbulence transport directly to gradients of the mean flow, it is not clear that they can adequately describe the complex interaction process sustained in the vicinity of the near wake. For example, in the near wake, the point of zero velocity gradient does not generally coincide with the point of zero shear. Also, it is not clear how much fluid dynamic detail is necessary to determine the aerodynamic performance of airfoil sections. Representative models of each type are considered in this study: (1) an algebraic eddy viscosity model of the type suggested by Smith and Cebeci,[1] which is modified by a relaxation formula in an attempt to account for upstream history effects, and (2) a Reynolds stress model of the type suggested by Bradshaw et al.[2] The Reynolds stress model is used in conjunction with the interaction hypothesis suggested by Bradshaw[3] in an attempt to deal directly with the interaction in the near-wake region. This model, relatively untested for asymmetric wakes, treats the near wake as a complex shear layer composed of two overlapping simple shear layers with shear profiles of opposite sign. This model accounts for upstream history effects in a natural manner and it is hoped it can support analyses of turbulent near wakes. By studying both models and retaining a rigorous set of equations and an adequate computational control volume, it may be possible to assess the sensitivity of airfoil computations to the details of the near-wake interaction and also assess the sensitivity of near-wake computations to the sophistication of the turbulence transport model.

Computations are made with the strong conservative form of the time-dependent compressible Navier-Stokes equations by using MacCormack's finite volume mixed

explicit/implicit/method-of-characteristics algorithm.[4] The equations are written and solved in Cartesian x-y space for computational meshes of arbitrary geometry. An exponentially stretched grid with thickness the order of the shear layer thickness is used to resolve the viscous flow regime. Near the solid surface, this grid is fine enough to resolve the viscous sublayer where velocity varies linearly with distance from the surface. Outside this viscous region, a second exponentially stretched grid is used to resolve the inviscid field to distances far from the body surface (typically 15 chord lengths). This kind of grid construction supports all the flow field features and also permits computational efficiency. To facilitate adequate resolution of the near wake, the computational grid is dynamically remeshed during the course of the solution so that the mesh always follows the path of the wake (as defined by the locus of minimum velocity). Solutions are advanced in time until a steady state is reached.

Detailed data is sparse for asymmetric near wakes. In this study, the RAE data reported by Cook[5] are compared with our computation. Measurements include boundary layer and wake pitot surveys and extracted skin friction and integral parameters. Comparisons are made with lift coefficient, pressure distribution, and velocity profiles.

Turbulence Models

Eddy viscosity models incorporate turbulent transport into the molecular transport stress tensor by adding the scalar eddy-viscosity transport coefficient ϵ, thereby relating turbulent transport directly to gradients of the mean-flow variables. In a Cartesian coordinate system, the two-dimensional molecular stress tensor can be written as

$$\tau_\ell = (p+\sigma_x)\vec{e}_x\vec{e}_x + \tau_{xy}\vec{e}_x\vec{e}_y + \tau_{yx}\vec{e}_y\vec{e}_x + (p+\sigma_y)\vec{e}_y\vec{e}_y \tag{1}$$

where the components are defined by

$$\sigma_x = -2\mu(\partial u/\partial x) - \lambda(\partial u/\partial x + \partial v/\partial y) \tag{2}$$

$$\sigma_y = -2\mu(\partial v/\partial y) - \lambda(\partial u/\partial x + \partial v/\partial y) \tag{3}$$

$$\tau_{xy} = \tau_{yx} = -\mu(\partial u/\partial y + \partial v/\partial x) \tag{4}$$

and

$$\lambda = -2\mu/3$$

The total shear (molecular plus turbulent) is written as

$$\tau = \tau_\ell + \tau_t = (p+\tilde{\sigma}_x)\vec{e}_x\vec{e}_x + \tilde{\tau}_{xy}\vec{e}_x\vec{e}_y + \tilde{\tau}_{yx}\vec{e}_y\vec{e}_x + (p+\tilde{\sigma}_y)\vec{e}_y\vec{e}_y \tag{5}$$

where

$$\tilde{\sigma}_x = -2(\mu + \rho\epsilon)(\partial u/\partial x) - \lambda(\partial u/\partial x + \partial v/\partial y) \tag{6}$$

$$\tilde{\sigma}_y = -2(\mu + \rho\epsilon)(\partial v/\partial y) \quad \lambda(\partial u/\partial x + \partial v/\partial y) \tag{7}$$

$$\tilde{\tau}_{xy} = \tilde{\tau}_{yx} = -(\mu + \rho\epsilon)(\partial u/\partial y + \partial v/\partial x) \tag{8}$$

In a similar manner, turbulent heat transport is defined in terms of mean energy gradients and an eddy conductivity coefficient k_t so that

$$Q_t = k_t \nabla T \tag{9}$$

Typically, the eddy conductivity coefficient is related to the eddy viscosity coefficient via a turbulent Prandtl number Pr_t where

$$Pr_t = \rho\, c_p\, \epsilon/k_t \tag{10}$$

The simplest eddy viscosity models are algebraic. In our examples, we used an algebraic model of the type suggested by Smith and Cebeci where in the boundary layer near the solid surface we have

$$\epsilon = \ell^2[(\partial u/\partial y)^2 + (\partial v/\partial x)^2]^{\frac{1}{2}} \tag{11}$$

$$\ell = 0.4\,\eta[1 - \exp(-\eta/A)] \tag{12}$$

$$A = 26\,\mu_w/\sqrt{\rho_w \tau_w} \tag{13}$$

and in the outer part of the boundary layer and in the wake we have

$$\epsilon = 0.0168\,\hat{u}_\delta \delta_1^*/\{1 + 5.5[(\eta - \eta_{DS})/\delta]^6\} \tag{14}$$

$$\delta_1^* = \int_{\eta_{DS}}^{\delta} (1 - \hat{u}/\hat{u}_\delta)\,d\eta \tag{15}$$

To approximate the influence of upstream history a simple relaxation procedure is used such that

$$\epsilon(\xi, \eta) = \alpha\epsilon(\xi - \Delta\xi, \eta) + (1 - \alpha)\,\epsilon_{eq}(\xi, \eta) \tag{16}$$

where ϵ_{eq} is defined by equations (11) and (14), α is a relaxation parameter with value between zero and one and $\Delta\xi$ is the local streamwise computational mesh spacing. For $\alpha = 0$, there is no relaxation and for $\alpha = 1$, the eddy viscosity is frozen. A value of 0.3 is used for α in the examples. The turbulent Prandtl number is assumed constant at 0.90.

This model has been used in previous studies[6,7] and found to support complex interacting flows reasonably well qualitatively. However, it is doubtful that a model developed for boundary layers and wakes will describe the complex turbulent mixing in the near wake of lifting airfoils.

Reynolds stress models require separate transport equations to describe the components of the Reynolds stress tensor. Their dependence on the mean flow gradients is indirect as opposed to the direct dependence in eddy coefficient models. The simplest Reynolds stress model is the one-equation, thin-shear-layer model. In this example, the thin-shear-layer Reynolds stress model proposed by Bradshaw *et al.*[2] is considered. The turbulent transport in the near wake is described using the interaction hypothesis formulated by Bradshaw *et al.*[3] This concept was first applied to symmetric wakes by Morel and Torda[8] and more recently by Huffman and Ng.[9] In this approach, the two shear layers from the upper and lower surfaces are considered as separate and distinct "simple" shear layers. Experiments[10] indicate that, in the near wake, the shear layers interact with each other only in a very thin interfacing region. For the most part, they continue to behave as a flow in which the shear stress does not change sign and which has one set of large eddies only. These two simple shear layers then "time share" an ever increasing region as they progress downstream from the trailing edge. Figure 1 is a schematic illustration of the free interaction concept in the near-wake region. The resultant shear stress in the interaction region can be determined by superposing the stresses resulting from the two simple shear layers. The attractive feature of such a concept is that the complex flow should not be very different from those for the corresponding simple shear layers alone.

The transport equation for Reynolds stress is written in a coordinate system corresponding to the thin shear layer as

$$\frac{\partial \tau^+}{\partial t} + \frac{\partial \hat{u}\tau^+}{\partial \xi} + \frac{\partial \hat{v}\tau^+}{\partial \eta} = c^+\tau^+\left(\frac{\partial \hat{u}}{\partial \eta} - \frac{\sqrt{|\tau^+/\rho|}}{L^+}\right) - \frac{\partial \tau^+ V_\tau^+}{\partial \eta} \tag{17}$$

where $\tau^+ = -\rho\,\overline{\hat{u}'\hat{v}'}$

The term $c^+\tau^+\partial\hat{u}/\partial\eta$ represents generation (sometimes called production), $-c^+\tau^+\sqrt{|\tau^+/\rho|}/L^+$ represents destruction (dissipation), and $-\partial\tau^+V_\tau^+/\partial\eta$ is transport by bulk diffusion.

For certain types of simple shear flows, universal functions have been proposed for c^+, L^+ and V_τ^+. Generally, c^+ is assumed constant and equal to 0.30. Typically, it represents twice the ratio of shear stress τ^+ to turbulent kinetic energy. For boundary layer flows Bradshaw *et al.*[2] suggest the functions shown in figure 2 for L^+ and G where

$$V_\tau^+ = c^+\sqrt{|\tau^+/\rho|_{max}}\,G \tag{18}$$

These functions are represented analytically in the present study by the following relations:

$$L^+/\delta = \begin{cases} 0.40\ \eta/\delta & , \quad \eta/\delta \le 0.1818 \\ 0.04 + 0.22(1-\eta/\delta)\eta/\delta & , \quad 0.1818 < \eta/\delta \le 1.10 \\ 816.5\ \exp(-9.866\ \eta/\delta) & , \quad \eta/\delta > 1.10 \end{cases} \tag{19}$$

$$G\hat{u}_\delta/\sqrt{|\tau^+/\rho|_{max}} = \begin{cases} (1.117 + 16.94\ \eta/\delta)\eta/\delta & , \quad \eta/\delta < 0.6286 \\ 90.87\ \eta/\delta - 49.73 & , \quad 0.6286 \le \eta/\delta \le 0.895 \\ 18.69\ \eta/\delta + 14.86 & , \quad \eta/\delta > 0.895 \end{cases} \tag{20}$$

In this study, the length scale is modified for small values of η by a van Driest[11] damping term so that

$$L^+/\delta = 0.40(\eta/\delta)[1-\exp(-\eta/A)] \ , \quad \eta/A < 4.0$$

For fully developed wake flows Morel and Torda[8] suggest the functions shown in figure 3 for L and G. These functions are represented analytically in this study by the following relations

$$L^+/\delta = \begin{cases} 816.5\ \exp\{-9.866[1-(\eta/\delta)]\} & , \quad \eta/\delta < 0.07289 \\ 0.087 & , \quad 0.07289 \le \eta/\delta \le 0.92711 \\ 816.5\ \exp(-9.866\ \eta/\delta) & , \quad \eta/\delta > 0.97211 \end{cases} \tag{21}$$

$$G\,\Delta\,\hat{u}_{max}/\sqrt{|\tau^+/\rho|_{max}} = \begin{cases} -20 & , \quad \eta/\delta \le 0 \\ 34\ \eta/\delta - 20 & , \quad 0 < \eta/\delta < 0.2333 \\ 31\ \eta/\delta - 19.3 & , \quad 0.2333 \le \eta/\delta < 0.6636 \\ 20\ \eta/\delta - 12 & , \quad 0.6636 \le \eta/\delta < 0.9111 \\ 2\ \eta/\delta + 4.4 & , \quad \eta/\delta \ge 0.9111 \end{cases} \tag{22}$$

where $\Delta\,\hat{u}_{max}$ is the maximum velocity difference across the wake.

In the near wake, the empirical boundary-layer length and velocity functions are relaxed to the empirical functions for a fully developed wake using a relaxation length that is a multiple of the average of the two boundary layer thicknesses at the trailing edge. Hence, we have for the near wake

$$L^+/\delta = \mathscr{R}(L^+/\delta)_{BL} + (1-\mathscr{R})(L^+/\delta)_{WK} \tag{23}$$

$$V_\tau^+ = \mathscr{R}(V_\tau^+)_{BL} + (1-\mathscr{R})(V_\tau^+)_{WK} \tag{24}$$

$$\mathscr{R} = \exp(-\Delta\,\xi_{te}/\beta\,\bar{\delta}_{te}) \tag{25}$$

where $\Delta\,\xi_{te}$ is the distance from the trailing edge, $\bar{\delta}_{te}$ is the average of the upper and lower boundary-layer thicknesses, and β is the length scale multiplier. Experimental studies on turbulence relaxation length scales suggest a value of 10 for β, which was used in these studies.

To describe both shear layers simultaneously, two equations are necessary. Letting equation (17) represent the shear layer where the stress is positive we can write the stress equation for the shear layer where the stress is

negative as

$$\frac{\partial \tau^-}{\partial t} + \frac{\partial \hat{u}\tau^-}{\partial \xi} + \frac{\partial \hat{v}\tau^-}{\partial \eta} = c^-\tau^-\left(\frac{\partial \hat{u}}{\partial \eta} - \frac{\sqrt{|\tau^-/\rho|}}{L^-}\right) - \frac{\partial \tau^- V_\tau^-}{\partial \eta} \tag{26}$$

where $c^- = -c^+$, $L^-/\delta^-(\eta/\delta^-) = L^+/\delta^+(\eta/\delta^+)$, $V_\tau^- = c^-\sqrt{|\tau^-/\rho|_{max}}\,G$.

The Reynolds shear stress is then determined from the sum of the two components so that

$$-\rho\,\overline{\hat{u}'\hat{v}'} = -\rho\,\overline{\hat{v}'\hat{u}'} = \tau^+ + \tau^- \tag{27}$$

In regions where there is no interaction, e.g., boundary layers and the outer region of the wake, one component will be zero. Where there is an interaction between the two shear layers, as in the near wake, the superposition principle will apply.

The normal Reynolds stress components are approximated by

$$-\rho\,\overline{\hat{u}'^2} = -5(|\tau^+| + |\tau^-|) \tag{28}$$

$$-\rho\,\overline{\hat{v}'^2} = -2(|\tau^+| + |\tau^-|) \tag{29}$$

based on the assumptions that the turbulent kinetic energy is always partitioned 5:2 and that the ratio of shear to kinetic energy $c^+/2$ is approximately 1:7.

Reynolds analogy is used to relate the turbulent heat flux terms to the Reynolds stress components so that

$$-c_p\,\overline{\hat{v}'T'} = (\tau^+ + \tau^-)\,\gamma(\Delta e_i/\Delta\hat{u})_\delta \tag{30}$$

$$-c_p\,\overline{\hat{u}'T'} = -5(|\tau^+| + |\tau^-|)\,\gamma(\Delta e_i/\Delta\hat{u})_\delta \tag{31}$$

where $(\Delta e_i)_\delta$ and $(\Delta\hat{u})_\delta$ are the differences between the local values of e_i and $\hat{u}$ and their values at the outer edge of the shear layer.

In this initial study, no attempt is made to include extra rates of strain resulting from streamline curvature or other causes. These effects can be large and may be important in asymmetric near wakes when there is a strong viscous-inviscid interaction. Still to be studied, as well, is the consideration of a differential-length scale model. The application of the interaction hypothesis to near wakes is relatively recent and the inclusion of these additional levels of sophistication are perhaps best considered later one at a time.

Solution Procedure

The equations describing the flow field are written in integral form as

$$\frac{\partial}{\partial t}\int_{vol} U\,d\,vol + \int_S H\cdot\vec{n}\,ds = \phi\,vol \tag{32}$$

where for Cartesian momentum components

$$U = \begin{pmatrix} \rho \\ \rho u \\ \rho v \\ e \\ \hline \tau^+ \\ \tau^- \end{pmatrix}, \qquad H = \begin{pmatrix} \rho\vec{q} \\ \rho u\vec{q} + \tau\cdot\vec{e}_x \\ \rho v\vec{q} + \tau\cdot\vec{e}_y \\ e\vec{q} + \tau\cdot\vec{q} - k\nabla T - Q_t \\ \hline \tau^+\vec{q} \\ \tau^-\vec{q} \end{pmatrix} \tag{33,34}$$

$$\Phi = \begin{Bmatrix} 0 \\ 0 \\ 0 \\ 0 \\ \hline c^+\tau^+(\partial\hat{u}/\partial\eta - \sqrt{|\tau^+/\rho|}/L^+) - \partial\tau^+ V_\tau^+/\partial\eta \\ c^-\tau^-(\partial\hat{u}/\partial\eta - \sqrt{|\tau^-/\rho|}/L^-) - \partial\tau^- V_\tau^-/\partial\eta \end{Bmatrix} \tag{35}$$

The equations below the dashed line are considered only with the Reynolds stress model. They are written in terms of the curvilinear coordinate system corresponding to the thin shear layer where ξ is the streamwise direction and η is the transverse direction. Although the momentum components are written in the Cartesian coordinate system, the velocity and heat flux vectors are written in the curvilinear mesh coordinate system so that

$$\vec{q} = \hat{u}\vec{g}_\xi + \hat{v}\vec{g}_\eta \tag{36}$$

$$\nabla T = (\partial T/\partial\xi)\vec{g}_\xi + (\partial T/\partial\eta)\vec{g}_\eta \tag{37}$$

$$Q_t = \begin{cases} k_t \nabla T & , \quad \epsilon \text{ model} \\ (-c_p \overline{\hat{u}'T'})\vec{g}_\xi + (-c_p \overline{\hat{v}'T'})\vec{g}_\eta & , \quad \tau_t \text{ model} \end{cases} \tag{38}$$

The shear stress is given by equations (5) through (8) for the eddy viscosity model. For the Reynolds stress model $\tau = \tau_\ell - \tau_t$ where τ_ℓ is defined in equations (1) through (4) and

$$\tau_t = (-\rho \overline{\hat{u}'^2})\vec{g}_\xi\vec{g}_\xi + (-\rho \overline{\hat{u}'\hat{v}'})\vec{g}_\xi\vec{g}_\eta + (-\rho \overline{\hat{v}'\hat{u}'})\vec{g}_\eta\vec{g}_\xi + (-\rho \overline{\hat{v}'^2})\vec{g}_\eta\vec{g}_\eta \tag{39}$$

and the Reynolds stress components are defined by equations (27) through (29).

Equation (32) can be solved for arbitrary geometries with computational meshes of arbitrary configuration. For simplicity in treating the Reynolds stress equation, the coordinate system should be orthogonal and body oriented in the viscous region. This kind of coordinate system also simplifies the characteristic operator in the MacCormack[4] method used to solve the equations.

Constructing the transformation between Cartesian space and the computational space we have

$$\xi = \xi(x,y) \ , \quad \eta = \eta(x,y) \tag{40}$$

with a Jacobian of the transformation

$$J = (\partial x/\partial\xi)(\partial y/\partial\eta) - (\partial y/\partial\xi)(\partial x/\partial\eta)$$

The covariant base vectors can be written as

$$\left.\begin{aligned} \vec{g}_\xi &= (\partial x/\partial\xi)\vec{e}_x + (\partial y/\partial\xi)\vec{e}_y \\ \vec{g}_\eta &= (\partial x/\partial\eta)\vec{e}_x + (\partial y/\partial\eta)\vec{e}_y \end{aligned}\right\} \tag{41}$$

and the contravariant base vectors as

$$\left.\begin{aligned} \vec{g}^\xi &= (\partial\xi/\partial x)\vec{e}_x + (\partial\xi/\partial y)\vec{e}_y \\ \vec{g}^\eta &= (\partial\eta/\partial x)\vec{e}_x + (\partial\eta/\partial y)\vec{e}_y \end{aligned}\right\} \tag{42}$$

The transformation metrics are

$$\left.\begin{aligned} g_{\xi\xi} &= \vec{g}_\xi\cdot\vec{g}_\xi = (\partial x/\partial\xi)^2 + (\partial y/\partial\xi)^2 \\ g_{\eta\eta} &= \vec{g}_\eta\cdot\vec{g}_\eta = (\partial x/\partial\eta)^2 + (\partial y/\partial\eta)^2 \\ g_{\xi\eta} &= g_{\eta\xi} = (\partial x/\partial\xi)(\partial x/\partial\eta) + (\partial y/\partial\xi)(\partial y/\partial\eta) \end{aligned}\right\} \tag{43}$$

and

$$\left.\begin{aligned} g^{\xi\xi} &= \vec{g}^{\xi}\cdot\vec{g}^{\xi} = (\partial\xi/\partial x)^2 + (\partial\xi/\partial y)^2 \\ g^{\eta\eta} &= \vec{g}^{\eta}\cdot\vec{g}^{\eta} = (\partial\eta/\partial x)^2 + (\partial\eta/\partial y)^2 \\ g^{\eta\xi} &= g^{\xi\eta} = (\partial\xi/\partial x)(\partial\eta/\partial x) + (\partial\xi/\partial y)(\partial\eta/\partial y) \end{aligned}\right\} \tag{44}$$

For the computational coordinate system we can write equation (32) in differential form as

$$\frac{\partial U}{\partial t} + \frac{1}{L_i}\frac{\partial(H\cdot\vec{n}_\xi\,\Delta S_\xi)}{\partial\xi} + \frac{1}{L_j}\frac{\partial(H\cdot\vec{n}_\eta\,\Delta S_\eta)}{\partial\eta} = \Phi_{ij} \tag{45}$$

where $L_i = \mathrm{vol}_{ij}/\Delta\xi$, $L_j = \mathrm{vol}_{ij}/\Delta\eta$. The flux components can be written as

$$(H\cdot\vec{n}_\xi\,\Delta S_\xi) = J\Delta\eta \begin{bmatrix} \rho\hat{u} \\ \rho u\hat{u} + \tau\cdot\vec{e}_x\cdot\vec{g}^{\xi} \\ \rho v\hat{u} + \tau\cdot\vec{e}_y\cdot\vec{g}^{\xi} \\ e\hat{u} + \tau\cdot\vec{q}\cdot\vec{g}^{\xi} - k\nabla T\cdot\vec{g}^{\xi} - Q_t\cdot\vec{g}^{\xi} \\ \hline \tau^{+}\hat{u} \\ \tau^{-}\hat{u} \end{bmatrix} \tag{46}$$

$$(H\cdot\vec{n}_\eta\,\Delta S_\eta) = J\Delta\xi \begin{bmatrix} \rho\hat{v} \\ \rho u\hat{v} + \tau\cdot\vec{e}_x\cdot\vec{g}^{\eta} \\ \rho v\hat{v} + \tau\cdot\vec{e}_y\cdot\vec{g}^{\eta} \\ e\hat{v} + \tau\cdot\vec{q}\cdot\vec{g}^{\eta} - k\nabla T\cdot\vec{g}^{\eta} - Q_t\cdot\vec{g}^{\eta} \\ \hline \tau^{+}\hat{v} \\ \tau^{-}\hat{v} \end{bmatrix} \tag{47}$$

where

$$\vec{n}_\xi\,\Delta S_\xi = (\vec{g}^{\xi}/\sqrt{g^{\xi\xi}})(\sqrt{g_{\eta\eta}}\,\Delta\eta) = J\Delta\eta\,\vec{g}^{\xi} \tag{48}$$

and

$$\vec{n}_\eta\,\Delta S_\eta = (\vec{g}^{\eta}/\sqrt{g^{\eta\eta}})(\sqrt{g_{\xi\xi}}\,\Delta\xi) = J\Delta\xi\,\vec{g}^{\eta} \tag{49}$$

For computational efficiency in the viscous region, the term $(H\cdot\vec{n}_\eta\,\Delta S_\eta)$ is split into a parabolic part, which is treated implicitly, and a hyperbolic part, which is treated explicitly. Thus for the parabolic part we have

$$(H\cdot\vec{n}_\eta\,\Delta S_\eta)_P = J\Delta\xi \begin{bmatrix} 0 \\ (\tau - p)\cdot\vec{e}_x\cdot\vec{g}^{\eta} \\ (\tau - p)\cdot\vec{e}_y\cdot\vec{g}^{\eta} \\ (\tau - p)\cdot\vec{q}\cdot\vec{g}^{\eta} - k\nabla T\cdot\vec{g}^{\eta} - Q_t\cdot\vec{g}^{\eta} \\ \hline 0 \\ 0 \end{bmatrix} \tag{50}$$

and the hyperbolic part

$$(H\cdot\vec{n}_\eta\,\Delta S_\eta)_H = J\Delta\xi \begin{bmatrix} \rho\hat{v} \\ \rho u\hat{v} + p\vec{e}_x\cdot\vec{g}^{\eta} \\ \rho v\hat{v} + p\vec{e}_y\cdot\vec{g}^{\eta} \\ (e+p)\hat{v} \\ \hline \tau^{+}\hat{v} \\ \tau^{-}\hat{v} \end{bmatrix} \tag{51}$$

For the Bradshaw Reynolds stress model, there are no gradient diffusion terms and the model transport equations are hyperbolic. In practice, the bulk diffusion velocities V_τ^{+} and V_τ^{-} are combined with the convection velocity $\hat{v}$. The source term Φ then contains only the generation and destruction terms. This source term can lead to numerical instability if sufficient care is not exercised in its treatment. Linear stability analysis indicates the equations

are unconditionally unstable. In the steady state, an exact balance is maintained between generation, destruction, bulk diffusion, and convection. In the transient case, however, there will be regions in the flow where turbulence is being generated faster than it is being carried away or dissipated. Artificial constraints must be imposed on the magnitude of the generation and destruction terms so there is no unstable exponential growth or decay of the Reynolds stress. In this study, this is achieved by artifically limiting the magnitude of generation less destruction such that

$$|\partial\hat{u}/\partial\eta - \sqrt{|\tau/\rho|}/L| < 0.02/\Delta t$$

where Δt is the time advanced by the differential operator. Although some time accuracy is lost, the growth limitation is not altogether inconsistent with the implicit treatment of the other viscous terms.

In addition to the artificial constraint on the magnitude of Φ, the distribution of Φ across the shear layer is quadratically smoothed to minimize the development of unstable oscillations. To further minimize the chance of instability, an eddy viscosity transport model is used to obtain starting solutions, thus avoiding problems associated with a large initial transient change.

Mesh Construction

A computational mesh is constructed around the airfoil geometry as follows. First, an orthogonal body-oriented mesh is constructed around the airfoil (with the airfoil surface treated as one mesh line) and extended out a distance sufficient to capture the viscous-dominated flow region (typically a few percent of the chord length of the airfoil, say 10%). This mesh is extended downstream from the trailing edge of the airfoil (typically 15 chord lengths) at an angle relative to the mean chord line corresponding to the angle of attack of the airfoil to the oncoming stream. The mesh spacing normal to the airfoil surface is exponentially stretched with the first mesh spacing set equal to 1/12th of the chord length divided by the chord Reynolds number. There are 20-30 mesh points distributed across this viscous layer to the outer edge of the zone. Points are generated (or input) along the airfoil surface and distributed exponentially downstream in the wake to a maximum total of 100 "surface" points in the wake and on the airfoil. Second, a larger and coarser mesh is constructed extending from the outer edge of the viscous mesh to a distance far from the airfoil (typically 15 chord lengths). Again, exponential stretching is used away from the surface and some 20 to 30 points are distributed across the region. The radial mesh lines are required to be continuous with those in the viscous mesh, but the requirement of orthogonality is relaxed so that mesh lines neither converge (cross) nor diverge too rapidly. The mesh constructed for the RAE 2814 airfoil is shown in figure 4.

As the flow develops, the position of the viscous wake moves with time. To assure the capture of the wake in the viscous mesh, the mesh downstream from the trailing edge of the airfoil is dynamically adjusted during the course of the solution in a direction normal to the mean chord of the airfoil so that the slope of the wake mesh matches the flow direction in the core of the wake. This dynamic remeshing is initiated sometime after the impulsive start (typically after a dimensionless time of 1) to allow time for the starting vortex to be shed downstream. Mesh adjustment is realized gradually with the adjustment never exceeding the smallest transverse mesh spacing in any one time step.

Results

Computed results have been obtained for the RAE 2814 airfoil section corresponding to the test conditions of Cook[5] where the free stream Mach number is

0.725, the angle of attack is 1.44°, and the chord Reynolds number is 15×10^6. Solutions were generated from an inviscid impulsive start for a dimensionless time ($U_\infty t/c$) of approximately 0.2. The eddy viscosity model was then included and the no-slip boundary condition imposed, and the solution continued to a dimensionless time of 12. Comparisons of computed and experimental wake velocity profiles just aft of the trailing edge are shown in figure 5. In the first 10% of dimensionless downstream distance, the experimental data show fuller profiles from the upper surface than the computations, and less full profiles from the lower surface than the computations. Further downstream the agreement is quantitatively very good and symmetry is rapidly approached in both computation and experiment.

The computation was extended to a dimensionless time of 13 using the Reynolds stress model. Comparisons of computed velocity profiles in the near wake, obtained with eddy viscosity and shear stress models, are shown in figure 6. Just aft of the trailing edge, the Reynolds stress model solution yields an even less full upper layer profile and a fuller lower layer profile than the eddy viscosity model solutions. These differences diminish rapidly as the flow progresses downstream and, for the upper layer, the trend actually reverses. This suggests too large a Reynolds stress relaxation length in the central wake region. A length of 10 δ_{te} was used in the computations.

Figure 7 shows comparisons of near wake shear profiles for both the eddy viscosity and Reynolds stress computations. The distinctive difference in the two distributions appears in the central core of the wake where the eddy viscosity model exhibits large values of shear stress and a very large gradient where the stress changes sign. These large differences in turbulent shear distribution and magnitude, however, seem to have little effect on the mean velocity profiles, as shown in figure 6. The influence of these differences in shear distribution and magnitude is even less on the pressure distribution over the airfoil and in the near wake. Figure 8 is a comparison of computed and experimental surface-pressure distributions. Except for the vicinity of the trailing edge, the agreement between computation (with both turbulence models) and experiment is very good. There is some streamwise oscillation in the computed pressure distribution near the trailing edge and the values are typically smaller than the experimental results. The difference in magnitude of pressure coefficient is coupled with the velocity distributions at the trailing edge where the computed displacement thickness on the upper surface is greater than the experimentally determined thickness. Although the near-wake pressure prediction is slightly better using the Reynolds stress model, there is still room for further refinement before good quantitiatve agreement can be reached.

Concluding Remarks

A numerical scheme has been described to study interactive flows in the vicinity of two-dimensional near wakes. The Reynolds averaged Navier-Stokes equations are used to ensure proper treatment of viscous-inviscid interactions, and both eddy viscosity and Reynolds stress turbulence transport models are considered to describe the complex mixing in the viscous-viscous interaction region. Although differences in turbulent shear stress distributions in the near wake for the two different models appears to be large, the influence on pressure distribution and resulting lift and drag on the airfoil is small. The greatest source of disagreement between computed and experimental pressure distribution is related to the large computed displacement thickness just ahead of the trailing edge. More detailed turbulence transport models may be necessary in the wall-shear-flow region to realize improvement at the trailing edge.

References

1. Smith, A. M. O. and Cebeci, T.: "Numerical Solution of the Turbulent Boundary-Layer Equations," Douglas Aircraft Div., Report DAC 33735 (1967).
2. Bradshaw, P., Ferriss, D. H., and Atwell, N. P.: "Calculation of Boundary Layer Development using the Turbulent Energy Equation," J. Fluid Mech. 28, 593 (1967).
3. Bradshaw, P., Dean, R. B., and McEligot, D. M.: "Calculation of Interacting Turbulent Shear Layers. Duct Flow," J. Fluids Engr. 95, 214 (1973).
4. MacCormack, R. W.: "An Efficient Explicit-Implicit-Characteristic Method for Solving the Compressible Navier-Stokes Equations," SIAM-AMS Proceedings, XI (1978).
5. Cook, T. A.: "Measurements of the Boundary Layer and Wake of Two Aerofoil Sections at High Reynolds Number and High-Subsonic Mach Numbers," RAE Tech. Rept. 71127 (1971).
6. Deiwert, G. S.: "Computation of Separated Transonic Turbulent Flows," AIAA J. 14, No. 6, 735 (1976).
7. Deiwert, G. S.: "Recent Computation of Viscous Effects in Transonic Flow," Proc. V Int. Conf. on Numerical Methods in Fluid Dynamics, 59, Springer-Verlag, New York (1976).
8. Morel, T. and Torda, T. P.: "Calculation of Free Turbulent Mixing Layers by the Interaction Approach," AIAA J. 12 (1974).
9. Huffman, G. D. and Ng, B. S-H.: "Modeling of an Asymmetric Turbulent Near Wake Using the Interaction Hypothesis," AIAA J. 16, 193 (1978).
10. Andreopoulos, J.: "Symmetric and Asymmetric Near Wake of a Flat Plate," Ph.D. Thesis, Dept. of Aeronautics, Imperial College, London University (1978).
11. van Driest, E. R.: "On Turbulent Flow Near a Wall," J. Aero. Sci. 23, 1007 (1956).

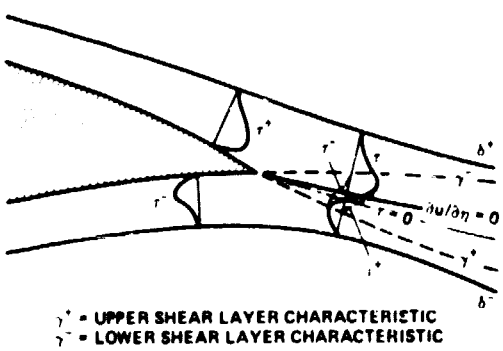

Fig. 1. Schematic of the overlapping shear layers at asymmetric trailing edge.

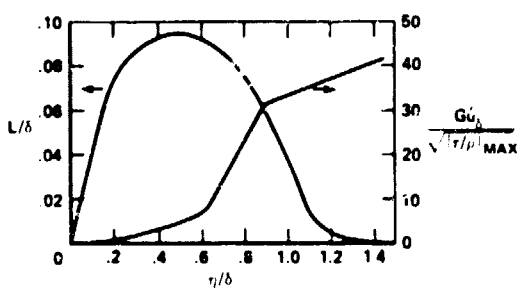

Fig. 2. Length and velocity scale functions for attached wall layers.

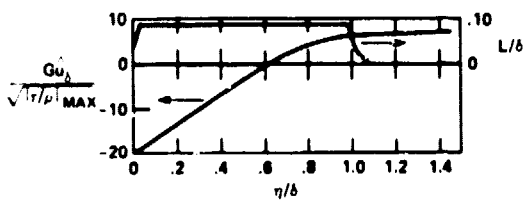

Fig. 3. Length and velocity scale functions for fully developed wakes.

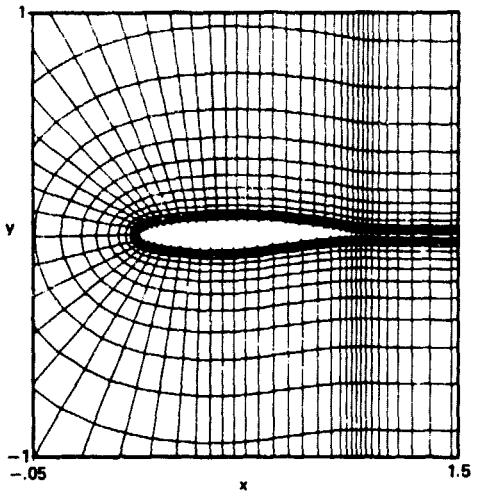

Fig. 4. Computational grid for RAE 2814 airfoil section.

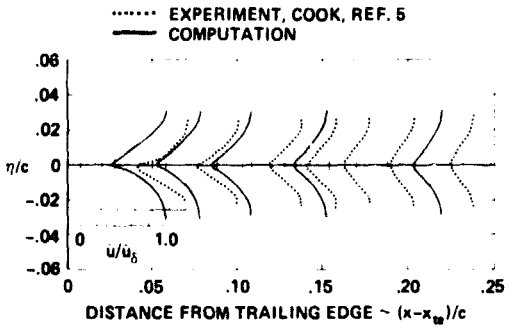

Fig. 5. Wake velocity profile development for RAE Section 2814; M = 0.725, α = 1.44, Re = 15 × 10^6.

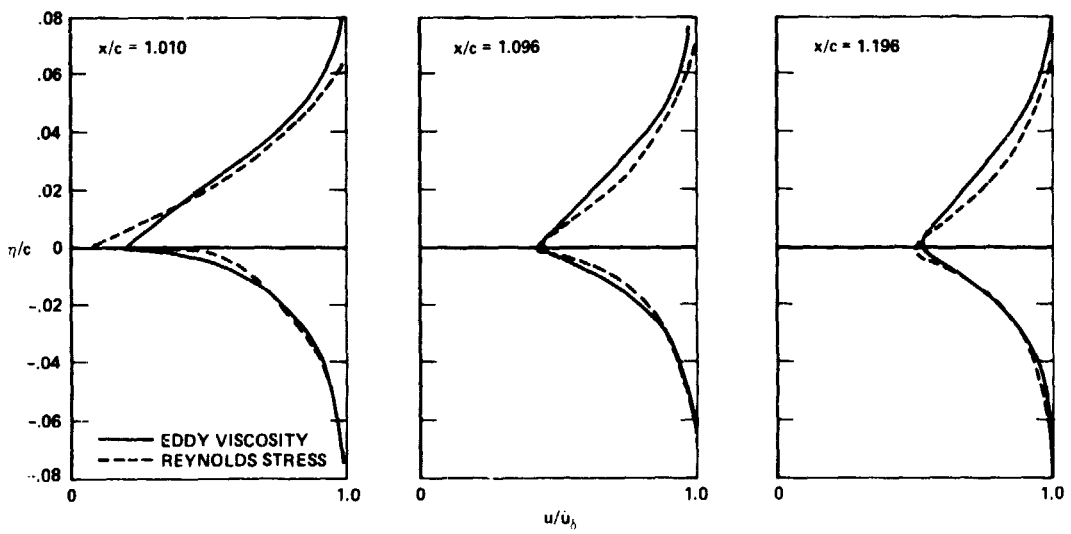

Fig. 6. Computed near-wake velocity profiles; eddy viscosity and Reynolds stress models.

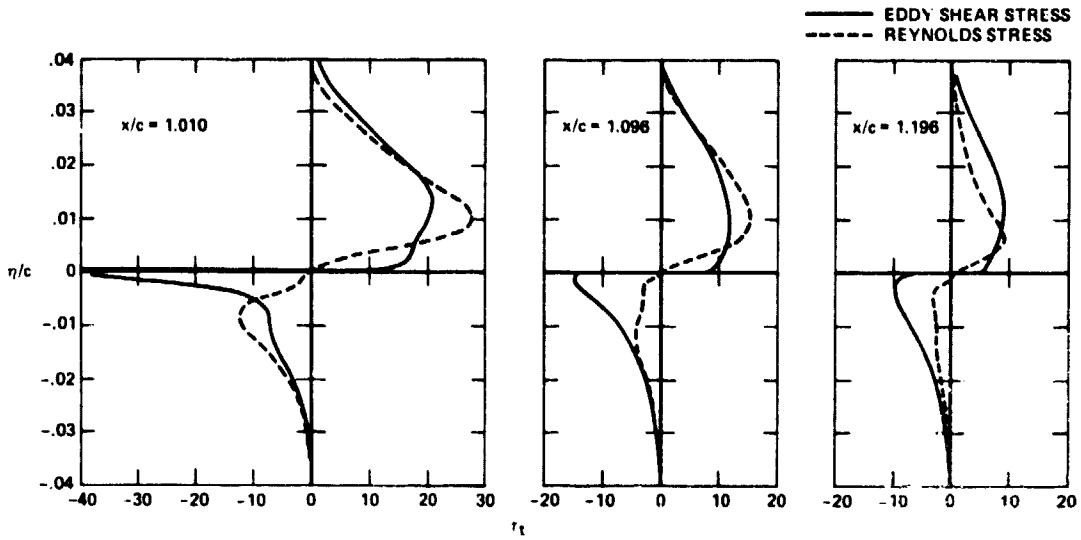

Fig. 7. Computed near-wake turbulent shear profiles; eddy viscosity and Reynolds stress models.

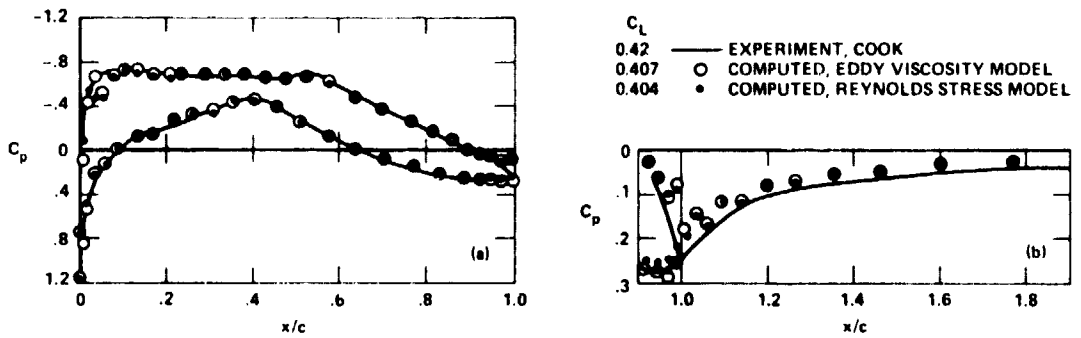

Fig. 8. Surface and near-wake pressure distributions for RAE Section 2814; M = 0.725, α = 1.44°, Re = 15 × 10^6. (a) Surface distribution. (b) Near-wake distribution.